Check for updates

Cetrimonium bromide and potassium thiocyanate assisted post-vapor treatment approach to enhance power conversion efficiency and stability of FAPbI₃ perovskite solar cells

Anjan Kumar, [ID] [ab] Sangeeta Singh,[b] Dilip Kumar Sharma,[c] Mohammed Al-Bahrani, [ID] *[d] Mohammed Ridha H. Alhakeem,[e] Amit Sharma[f] and T. Ch. Anil Kumar[g]

Formamidinium lead iodide (FAPbI₃) is the most promising perovskite material for producing efficient perovskite solar cells (PSCs). Here, we develop a facile method to obtain an α-phase FAPbI₃ layer with passivated grain boundaries and weakened non-radiative recombination. For this aim, during the FAPbI₃ fabrication process, cetrimonium bromide + 5% potassium thiocyanate (CTABr + 5% KSCN) vapor post-treatment is introduced to remove non-perovskite phases in the FAPbI₃ layer. Incorporation of CTA⁺ along with SCN⁻ ions induces FAPbI₃ crystallization and stitch grain boundaries, resulting in PSCs with lower defect losses. The vapor-assisted deposition increases the carriers' lifetime in the FAPbI₃ and facilitates charge transport at the interfacial perovskite/hole transport layer *via* a band alignment phenomenon. The treated α-FAPbI₃ layers bring an excellent PCE of 22.34%, higher than the 19.48% PCE recorded for control PSCs. Besides, the well-oriented FAPbI₃ and its higher hydrophobic behavior originating from CTABr materials lead to improved stability in the treated PSCs.

1. Introduction

Common perovskite solar cells now have recorded a high efficiency of 25.8%, thanks to their unique optoelectronic properties.[1,2] Perovskite materials with a small exciton binding energy are qualified for light harvesting tasks in solar cells. They quickly generate free photo carriers. Their high defect tolerance property guarantees the generation of a photo-current. Shockley–Queisser's theory indicates high-performance perovskite solar cells (PSCs) are accessible. But fabrication engineering is needed to avoid interfaces and bulk losses in the perovskite solar cell device and prepare highly efficient PSCs. Formamidinium lead iodide (FAPbI₃) perovskite with desirable photovoltaic properties has been used in

the literature to form efficient PSCs.[1,3–5] Highly crystalline, stable, and pure α-phase FAPbI₃ films are vital requirements for solar cell application. Usually, FAPbI₃ readily transfers from its photoactive α-phase to a photo-inactive δ-phase at temperatures lower than 150 °C.[4,6] Researchers have mixed FA⁺ cations with MA⁺, Cs⁺, K⁺, and Rb⁺ to address this issue and introduced new double, triple, and quadruple cation PSCs.[7–10] Mixed cation–anion perovskites while increasing the phase stability of FAPbI₃ perovskite generate other disadvantages such as low thermal stability, phase separation, and tight absorbance spectrum.[11–14] The broadened band-gap energy of mixed cation–anion perovskite systems reduces the number of photo-carriers and causes a lower photovoltaic performance in related PSCs than the pure FAPbI₃ PSCs. In addition, the incorporation of different cations with various ionic radii may induce a local strain and generate a distorted perovskite structure.[15,16]

In recent years, researchers developed new approaches to increase the phase stability of FAPbI₃ perovskite while keeping its optical and crystalline properties. Min *et al.*[4] incorporated methylenediammonium (MDA) cations into the FAPbI₃ structure to stabilize its α-phase. They showed forasmuch as ionic radii of MDA⁺ and FA⁺ are comparable, the absorbance edge position doesn't change, while more H groups of MDA⁺ induce ionic interaction and stabilize the α-phase of FAPbI₃. Lu *et al.* employed methylammonium thiocyanate (MASCN) vapor to

[a]CAD Lab, GLA University, Mathura-281406, India

[b]Microelectronics and VLSI Lab, National Institute of Technology (NIT), Patna-800005, India

[c]Department of Mathematics, Jaypee University of Engineering and Technology, Guna, M.P., India

[d]Chemical Engineering and Petroleum Industries Department, Al-Mustaqbal University College, Babylon, 51001, Iraq. E-mail: mohammed.naeem@mustaqbal-college.edu.iq

[e]Ministry of Oil, Midland Refineries Company, Baghdad, Iraq

[f]Department of Applied Sciences, Vidyapeeth's College of Engineering, A4, Paschim Vihar, New Delhi-110063, India

[g]Department of Mechanical Engineering, Vignan's Foundation for Science Technology and Research, Vadlamudi, Guntur Dt., Andhra Pradesh, India

convert the δ-phase to the desired α-phase. They found that SCN$^-$ ions promote the formation and stabilization of a-FAPbI$_3$. Jeong et al.[3] introduced formate anion (HCOO$^-$) to boost the α-FAPbI$_3$ crystallinity. They showed that HCOO$^-$ ions fill anion vacancies and brought a PCE of 25.6%. They proved that HCOO$^-$ ions have more binding affinity for iodide vacancies than the other halides of Cl$^-$, Br$^-$, and BF$_4^-$. Park et al.[17] added 15% of isopropylammonium chloride into the FAPbI$_3$ pre-solution and observed that remaining isopropylammonium cations at the grain boundaries (Gbs) assist in the stabilization of the α-FAPbI$_3$ structure. If organic ammonium halides employed as a passivation agent for surface treatment, not additive into the bulk of FAPbI$_3$, are good candidates for α-phase stabilization along with improving humidity stability. Liu et al.[18] used iso-butylammonium iodide to post-treat of FAPbI$_3$ perovskite. They found iso-butylammonium cations induce undesirable δ-FAPbI$_3$ to α-FAPbI$_3$ and also efficiently passivate electronic trap states near to the FAPbI$_3$ surface, improving the optoelectronic FAPbI$_3$ film. Jeong et al.[19] employed cyclohexylammonium iodide to passivate FAPbI$_3$ Gbs and form a 2D/3D heterostructure. They deduced that FA$^+$ ions on the 3D FAPbI$_3$'s surfaces are dissolved during the surface treatment, and cyclohexylammonium-based cations are reacted with the PbI$_2$ forming 2D perovskites over FAPbI$_3$ layer. Shen et al.[20] introduced sulfonyl fluoride-functionalized phenethylammonium (SF-PEA) salt as surface functionalization for a FAPbI$_3$ layer while maintaining its E_g value. They concluded SF-PEA not only passivates the surface defects but also protects the perovskite from phase transition.

The aforementioned discussions encouraged us to stabilize the α-phase of FAPbI$_3$ with a new strategy. Our method not only improves phase stability but also increases the humidity stability of the FAPbI$_3$ layer along with its photovoltaic efficiency. We exposed cetrimonium bromide + 5% potassium thiocyanate (CTABr + 5% KSCN) vapor to the FAPbI$_3$ layer during its fabrication process. The vapor post-treatment vanishes δ-phase in the FAPbI$_3$ layer. Introduction of CTA$^+$ along with SCN$^-$ ions stitch Gbs in the FAPbI$_3$ layer, resulting in PSCs with lower defect losses. The vapor post-treatment boosts the carriers' lifetime in the FAPbI$_3$ and facilitates charge transport with a band alignment phenomenon. The vapor-treated PSCs bring a champion efficiency of 22.34%, higher than the 20.11% efficiency obtained for control PSCs. In addition, the stabilized and hydrophobic α-FAPbI$_3$ PSCs show an improved stability behavior.

2. Experimentals

2.1. Deposition of hole blocking titanium dioxide (h-TiO$_2$) layer

In vial A, 10 mL of isopropyl alcohol (IPA, ≥99.7%, Sigma Aldrich) and 70 μL HCl (2 M) are mixed for 20 min in an ice bath. In vial B, 750 μL of tetraisopropyl orthotitanate (TTIP, ≥97%, Sigma Aldrich) is mixed with 10 mL of IPA for 20 min in the ice bath. Vial A solution is dropwise added into vial B. The final solution is stirred in the ice bath for 20 min and a further 15 min at room temperature (RT). The obtained solution is filtered with a 0.2 μm PTFE filter. 60 μL of the filtered solution is poured on pre-patterned FTO and spin-coated at 2000 rpm for 30 s. h-TiO$_2$ layers are dried in an oven at 100 °C for 5 min and then baked for 30 min at 450 °C.

2.2. Deposition of mesoporous titanium dioxide (m-TiO$_2$) layer

400 mg of titanium dioxide paste (MPT-20 Titania Paste, Greatcell Solar) is diluted with 2652 mg of ethanol (EtOH, 99.9%, Merck) and 75 mg of terpineol (Merck, 98%). The obtained solution is stirred overnight at RT. 75 μL of m-TiO$_2$ pre-solution is dropped on the h-TiO$_2$ layer and spin-coated at 3000 rpm for 25 s. After the spin-coating process, mtp layers are dried at a temperature of 100 °C for 5 min and sintered for 60 min at 500 °C.

2.3. Deposition of perovskite layer

Formamidinium lead triiodide (FAPbI$_3$) pre-solution is synthesized as follows. At first, 737.2 mg of lead iodide (PbI$_2$, 99.999%, Sigma Aldrich) is dissolved in 890 μL of N,N-dimethylformamide (DMF, 99.8%, Sigma Aldrich) and 110 μL of dimethyl sulfoxide (DMSO, 99.9%, Sigma Aldrich). The PbI$_2$ solution is stirred at 75 °C for 45 min and then is cooled down to RT. In the following, 275.2 mg formamidinium iodide (FAI, 99.99%, Greatcell solar) and 33 mg methylammonium chloride (MACl, 99.99%, Greatcell solar) are poured into the cooled PbI$_2$ solution, followed by stirring at RT for 30 min. 80 μL of FAPbI$_3$ pre-solution is spin-coated on the m-TiO$_2$ layer with a speed of 1000 rpm for 3 s and then 6000 rpm for 30 s. During the second step, 150 μL chlorobenzene (CB, 99.9%, Sigma Aldrich) anti-solvent is poured on the FAPbI$_3$ layer to assist the perovskite crystallization process. FAPbI$_3$ perovskite layers are post-annealed at 100 °C for 1 min and 155 °C for 15 min.

2.4. Vapor-assisted deposition (VAD)

FAPbI$_3$ layers are treated with a cetrimonium bromide (CTABr, 99%, Sigma Aldrich) + x(0–10)% potassium thiocyanate (KSCN, 99%, Sigma Aldrich) vapor during the fabrication process to improve the surface quality. For this aim, 5 mg of CTABr + x% KSCN materials are heated at 250 °C and its vapor is guided toward the pre-annealed FAPbI$_3$ layer for 10 min. It should be mentioned the addition of KSCN is in a weight ratio of CTABr. Temperature of 250 °C was chosen to heat the powders to guarantee decomposition of both CTABr and KSCN materials. To better insight, TGA curve of CTABr-5% KSCN powder has been shown in Fig. 1. Before employing VAD treatment, perovskite layers are first post-annealed at 100 °C for 1 min and 155 °C for 8 min, then vapor directed toward them.

2.4.1 Deposition of hole transport layer. 2,2′,7,7′-Tetrakis(N,N-di-p-methoxyphenylamino)-9,9′-spirobifluorene (spiro-OMeTAD, 99.8%, Lumtec) as a hole transfer material (HTM) is dissolved in CB to prepare a 40 mg mL^{-1} solution. The spiro-OMeTAD solution is doped with 39 μL of 4-tert-butylpyridine (tBP, 98%, Sigma Aldrich), 23 μL of bis(trifluoromethylsulfonyl) amine lithium (Li-TFSI, 99.95%, Sigma Aldrich) stock solution in acetonitrile (ACN, 99.8%, Sigma Aldrich) (516 mg mL^{-1}), and
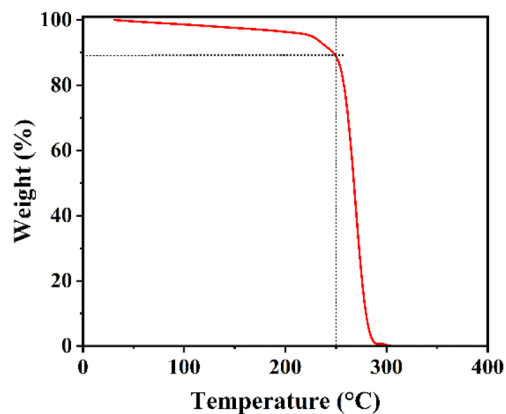
Fig. 1 TGA test of CTABr-5% KSCN powder at rate of 10 °C min^{-1}.

10 μL of stock solution of tris(2-(1*H*-pyrazol-1-yl)-4-*tert*-butyl-pyridine)-cobalt(III)tris(bis(trifluoromethylsulfonyl)imide) (FK209 Co(III) TFSI, 99%, Lumtec) in ACN (400 mg mL^{-1}). 70 μL of spiro-OMeTAD pre-solution is deposited on the FAPbI$_3$ perovskite layer by spin-coating at speed of 4000 rpm for 30 s. To study humidity stability of devices, poly[bis(4-phenyl)(2,4,6-trimethylphenyl)amine] (PTAA, Lumtec) is used as HTM. 15 mg of the PTAA material is dissolved in 1 mL of toluene (99.8%, Sigma Aldrich) contains 5 mol% of a tris(penta-fluorophenyl)borane (BCF, 98%, TCI) additive. 70 μL of PTAA solution is spin-coated over the FAPbI$_3$ layer with a speed of 3000 rpm.

2.5. Deposition of back electrodes

To complete the perovskite solar cell structure, gold electrodes with a thickness of 80 nm are thermally evaporated over the HTM layers at a high vacuum level with a controlled deposition rate of 1 Å s^{-1}.

2.6. Measurements

FAPbI$_3$ X-ray diffraction (XRD) patterns were investigated *via* a Brucker XRD spectrometer (D2 Phaser). Perovskite morphologies were monitored by FE-SEM micrographs recorded by Mira3, TESCAN FE-SEM equipment. Ultraviolet-visible absorbance spectrum of FAPbI$_3$ films was measured *via* a UV-2600i spectrometer (Shimadzu). A HORIBA Fl-1039/40 Fluorolog spectrometer was employed to collect the photoluminescence (PL) emission of excited FAPbI$_3$ layers with a 450 nm diode laser. Time-resolved PL (TRPL) decay traces of FAPbI$_3$ films on the glass substrate were collected at 805 nm with Horiba Fluorolog single photon counting system with exciting the FAPbI$_3$ films with a 532 nm pulsed laser excitation. The current–voltage (*I–V*) responses of FAPbI$_3$ solar cells under simulated illumination of AM 1.5G were conducted with a source meter (Keithley 2400). The active area of solar cells for *I–V* measurements was 0.1 cm^2. A calibrated Oriel ClassAAA solar simulator was employed as a light source for *I–V* tests. Capacitance–voltage (*C–V*) tests were measured *via* a VMP3, Biologic potentiometer device at a constant 10 kHz frequency from −0.2 to 1.1 V to gain

the Mott–Schottky curves. UPS of FAPbI$_3$ films was measured using a Thermo Fisher ESCALAB 250XL instrument with a monochromatic 21.22 eV He I light source.

3. Results

Here, we introduce an efficient method to vanish the photo inactive FAPbI$_3$ phase. In addition, the suggested approach boosts the photovoltaic (PV) efficiency and stability of FAPbI$_3$ PSCs. As shown in Fig. 2, the CTABr material is vaporized over the FAPbI$_3$ layer during the fabrication process. In continue, to further improve the PV performance of PSCs, the KSCN material as an additive is employed for the CTABr. In this step, different CTABr + x% KSCN ($x = 0$–7.5) mixed materials are prepared and vapor-treated the FAPbI$_3$ layers. Later, more discussion is involved to clarify the vapor-treatment effects on FAPbI$_3$ PSCs. From here onwards, untreated, treated with a vapor of CTABr, and treated with a vapor of CTABr-5% KSCN perovskite layers are labeled with control, CTABr-0%, and CTABr-5%, respectively. Fig. 2 schematically shows our employed method to fabricate different FAPbI$_3$ layers.

Fig. 3(a) shows absorbance spectra of control, CTABr-0%, and CTABr-5% FAPbI$_3$ films. Fig. 3(b) illustrates related Tauc curves to measure band-gap energy (E_g) of different FAPbI$_3$ layers. It is observed that vapor post-treated CTABr-5% FAPbI$_3$ has the highest light harvesting behavior than the control and CTABr-0% perovskite layers. Therefore, the CTABr-5% layer has the potential to record higher photo-current in related FAPbI$_3$ PSCs. In addition, Tauc plots represent a light blue shift in E_g value from 1.53 eV to 1.54 eV after conducting vapor post-treatment with CTABr or CTABr + 5% KSCN. It could be due to the slight diffusion of bromine ions (Br$^-$) and or thiocyanate ions (SCN$^-$).[21,22] Steady-state photoluminescence (PL) curves of different FAPbI$_3$ layers have been shown in Fig. 3(c). Responses show an increment in the intensity of PL peak for the CTABr-5% layer compared to the CTABr-0% and control FAPbI$_3$ layers, suggesting the prevented non-radiative charge recombination.[23,24] Later would be shown that the surface passivation caused by vapor treatment is a reason for the lower non-radiative charge recombination in the CTABr-5% FAPbI$_3$ layer. The collected X-ray diffraction (XRD) patterns of FAPbI$_3$ perovskite layers are shown in Fig. 3(d) to study the effects of vapor treatment on the FAPbI$_3$ crystalline properties. XRD patterns show two main peaks at $2\theta = 14.07°$ and $28.21°$ corresponding to (001) and (002) plane orientation of the α-FAPbI$_3$ phase.[3] It indicates the addition of 35 mol% of MACl forms well-oriented perovskite layers. In diffracted XRD peaks of the control layer, an additional peak at $2\theta = 11.59°$ assigned to the δ-FAPbI$_3$ phase is observed, while it is removed in the treated FAPbI$_3$ layers with vapors. In addition, the vapor of CTABr + 5% KSCN more effectively intensifies XRD signals and increases FAPbI$_3$ crystallinity.[25] We monitored full width at half maximum (FWHM) of (001) XRD peak for all layers. Fitted values of 0.1202, 0.1039, and 0.0981 were obtained for the control, CTABr-0%, and CTABr-5% FAPbI$_3$ layers, respectively. It indicates that vapors of CTABr and CTABr + 5% KSCN increase FAPbI$_3$ grains size.[26,27]

FESEM micro-images of FAPbI$_3$ layers are depicted in Fig. 4 to investigate their micromorphology. Fig. 4(a) shows the control layer has miro-sized grains with obvious grain boundaries (Gbs). Exposing CTABr vapor on the FAPbI$_3$ during the fabrication process enlarged perovskite grains, leading to lower surface defects in the FAPbI$_3$ layer (Fig. 4(b)). Employing the mixed vapor of CTABr + 5% KSCN further enlarged the perovskite grain (Fig. 4(c)). CTABr + 5% KSCN vapor well-passivated Gbs and reduced charge accumulation center in the FAPbI$_3$ surface. The enlarged perovskite grains reveal better photocarriers extraction at the perovskite/HTL interface and assist in the performance improvement of PSCs. Indeed, the passivated Gbs along with enlarged grains in the CTABr-5% FAPbI$_3$ layer are responsible for the boosted light-harvesting (see Fig. 3(a)) and the reduced non-radiative charge recombination (see Fig. 3(c)) observed in it.

In the following, we fabricated FAPbI$_3$ PSCs with or without vapor treatment steps to investigate the effects of vapors on the PV properties of PSCs. The calculated PV parameters from J–V characterizations are listed in Table 1. J–V curves of best-performance PSCs in each group of control, CTABr-0%, and CTABr-5% are depicted in Fig. 5(a). For the control PSCs, maximum efficiency of 19.48% with an open-circuit voltage (V_{OC}) of 1.110 V, a filling factor of 79.63%, and a short-circuit current density (J_{SC}) of 21.58 mA cm^{-2} was recorded. By applying CTABr vapor on the FAPbI$_3$ perovskite layer, the efficiency of FAPbI$_3$ PSCs reached up to 20.49% assigned to a V_{OC} of 1.130 V, a FF of 80.69%, and a J_{SC} of 22.47 mA cm^{-2}. Fig. 5(b–e) show statistical distribution of fabricated solar cells in each

group to find information on reproducibility of fabrication process. As listed results in Table 1 show, among vapors of CTABr + 2.5%, 5%, 7.5% KSCN, CTABr + 5% KSCN vapor forms more desirable FAPbI$_3$ for PV application and give raises higher PV parameters. By exposing CTABr + 5% KSCN on the FAPbI$_3$ layers, a champion efficiency of 22.05% assigned to a V_{OC} of 1.170 V, a FF of 82.11%, and a J_{SC} of 22.95 mA cm^{-2} was recorded for CTABr-5% PSCs. Fig. 5(f) shows the IPCE spectrum for different FAPbI$_3$ PSCs. The integrated J_{SC} are 21.47, 21.88, and 22.54 mA cm^{-2} for the control, CTABr-0%, and CTABr-5% FAPbI$_3$ PSCs, respectively. The integrated J_{SC} from IPCE spectra are in agreement with J_{SC} recorded from the J–V tests (see Table 1).

To find origin of PV improvements, TRPL, C–V, and UPS tests were conducted. Fig. 6(a) shows TRPL of different FAPbI$_3$ layers to investigate their charges lifetime. TRPL decay plots are fitted with a bi-exponential equation, as follow:

$$I(t) = A_1 \exp\left[\frac{-t_1}{\tau_1}\right] + A_2 \exp\left[\frac{-t_2}{\tau_2}\right] \quad (1)$$

In eqn (1), τ_1 and τ_2 indicate the fast and slow decay times. A_1 and A_2 indicate the fast and slow decay amplitudes. The average carrier lifetime (τ_{avg}) is calculated using $\tau_{avg} = \dfrac{\sum_{i=1}^{n} A_i \tau_i^2}{\sum_{i=1}^{n} A_i \tau_i}$ formula. Carrier lifetimes and amplitudes were listed in Table 2. τ_{avg} of 713.94, 1324.34, and 1675.31 ns were measured for the control,
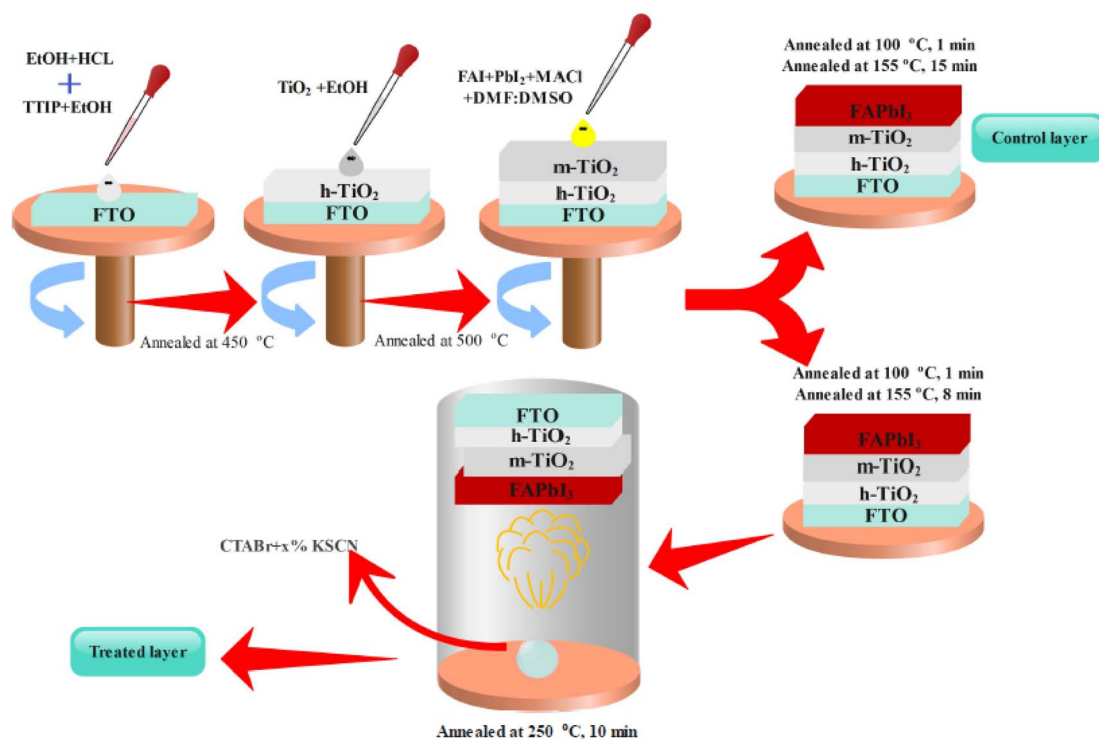

Fig. 2 Schematic view for fabrication of control and vapor treated FAPbI$_3$ layers.
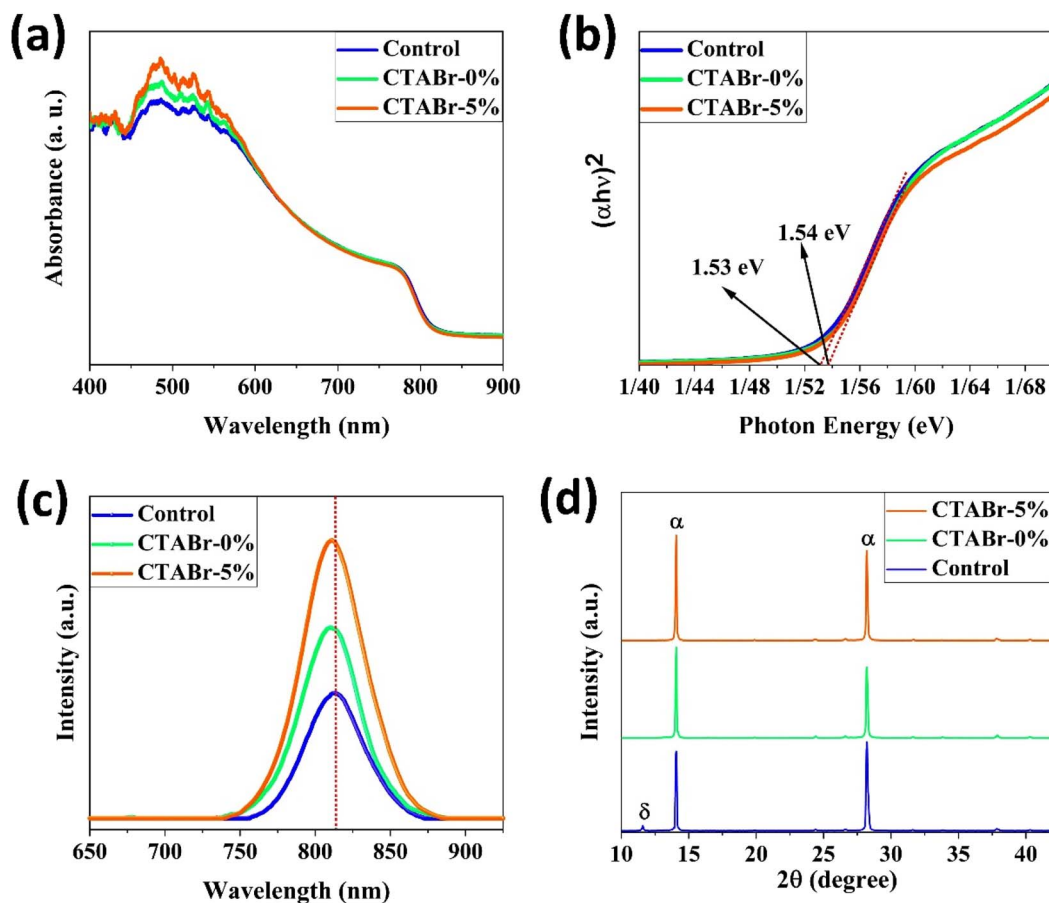
Fig. 3 (a) Ultraviolet-visible absorbance spectra, (b) related Tauc curves, (c) photoluminescence spectra, and (d) X-ray diffraction patterns of different FAPbI$_3$ layers.
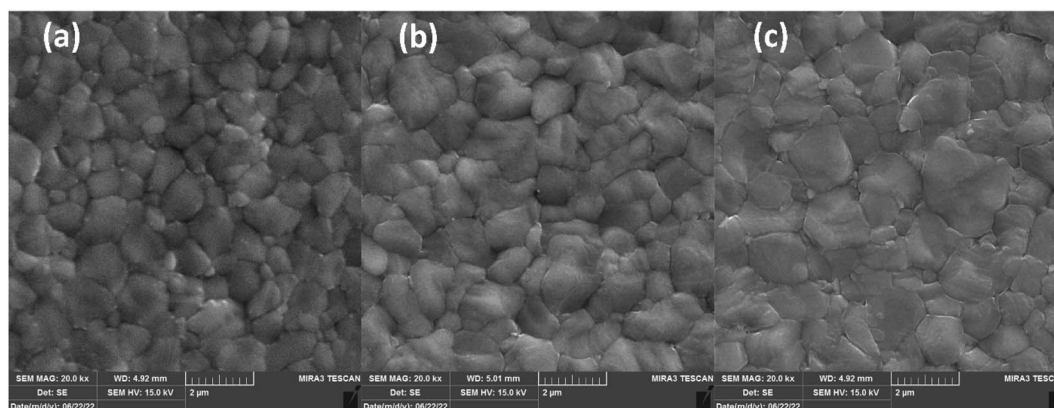

Fig. 4 FESEM micro-images of (a) control, (b) CTABr-0%, and (c) CTABr-5% vapor-treated FAPbI$_3$ layers.

CTABr-0%, and CTABr-5% FAPbI$_3$ layers, respectively. The fast decay is related to non-radiative charge recombination due to deep charge trapping in the FAPbI$_3$ layer. Slow decay refers to free carriers' radiative recombination processes.[15,28] Both τ_1 and τ_2 with vaporizing of CTABr over the control layer are increased, and with the assistance of KSCN, these values are further

boosted. The increased carrier lifetime refers to reduced non-radiative charge recombination by reducing the trap states in the FAPbI$_3$.[29] In addition, as summarized results in Table 2 show, employing vapor treatment reduces the A_1 proportion in the TRPL profile of the FAPbI$_3$ layer. It connotes reduced structural defects in the perovskite layer, consistent with the

Table 1 J–V photovoltaic values of FAPbI$_3$-based solar cells post-treated with different vapors of cetrimonium bromide + x% potassium thiocyanate (CTABr-x%)

| Device name		V_{OC} (V)	J_{SC} (mA cm^{-2})	FF (%)	PCE (%)
Control	Average	1.098 ± 0.019	21.58 ± 30	78.52 ± 0.80	18.61 ± 0.51
	Best	1.110	22.04	79.63	19.48
CTABr-0.0%	Average	1.116 ± 0.016	21.89 ± 0.37	79.99 ± 0.49	19.55 ± 0.53
	Best	1.130	22.47	80.69	20.49
CTABr-2.5%	Average	1.128 ± 0.020	22.38 ± 0.19	80.60 ± 0.52	20.35 ± 0.45
	Best	1.150	22.62	80.75	21.01
CTABr-5.0%	Average	1.152 ± 0.015	22.49 ± 0.32	82.10 ± 0.43	21.27 ± 0.51
	Best	1.170	22.95	82.11	22.05
CTABr-7.5%	Average	1.148 ± 0.015	22.37 ± 0.43	80.41 ± 0.67	20.66 ± 0.68
	Best	1.170	23.05	80.57	21.72
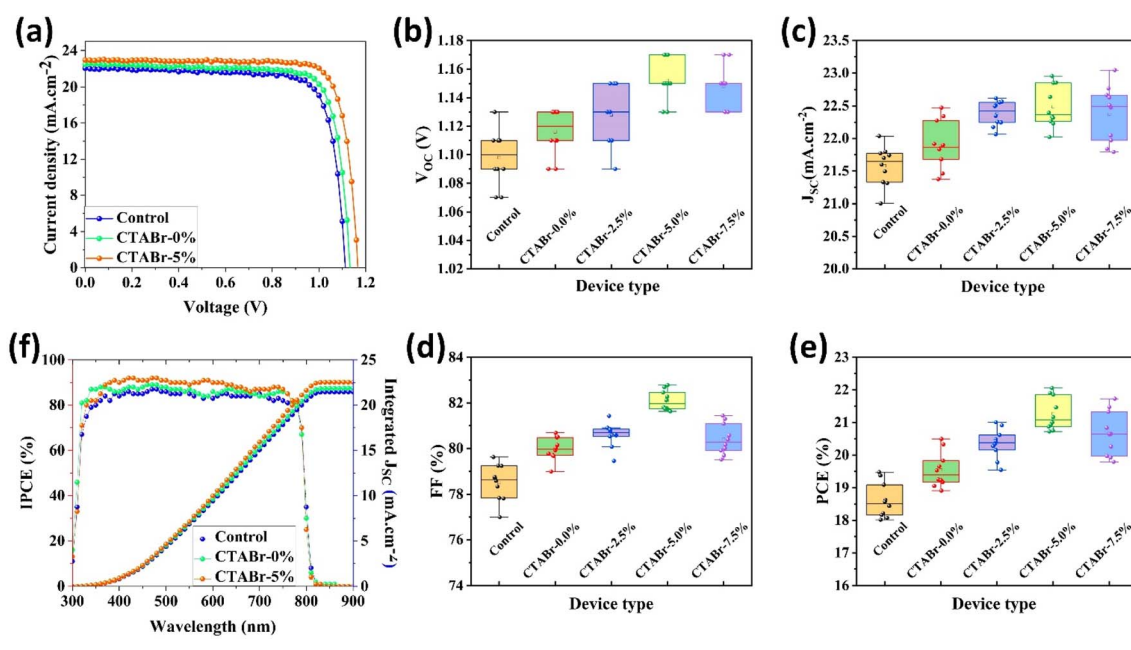
Fig. 5 (a) J–V curves of best-performance of different FAPbI$_3$-based solar cells. Box statistical distribution of (b) open-circuit voltage (V_{OC}), (c) short-circuit current density (J_{SC}), (d) fill factor (FF) and (e) power conversion efficiency (PCE) for different perovskite solar cells. (f) Incident photon-to-current efficiency curves of solar cells and related integrated current densities.
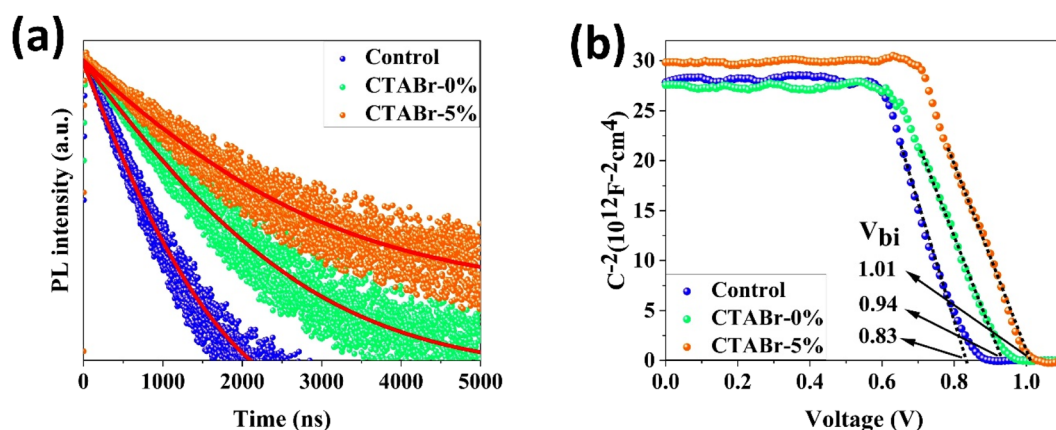
Fig. 6 (a) Time-resolved photoluminescence of FAPbI$_3$ films coated on glass substrates. Red solid lines indicate curves fitting with a bi-exponential equation. (b) Mott–Schottky curves of FAPbI$_3$ solar cells based on different FAPbI$_3$ layers.

Table 2 The results obtaining from the fitting of the time resolve photoluminescence of the control, CTABr-0%, and CTABr-5% for-mamidinium lead iodide (FAPbI₃) layers on the glass substrates. Control, CTABr-0%, and CTABr-5% allude to untreated, cetrimonium bromide vapor-treated, and cetrimonium bromide + 5% potassium thiocyanate treated FAPbI₃ layers

Perovskite	τ_1 (ns)	A_1 (%)	τ_2 (ns)	A_2 (%)	τ_{avg} (ns)
Control	09.54	16.50	0715.81	83.50	0713.94
CTABr-0%	17.00	13.57	1326.97	86.43	1324.34
CTABr-5%	19.55	08.38	1677.07	91.62	1675.31

Table 3 The band structure parameters of control, CTABr-0%, and CTABr-5% FAPbI₃ layers. E_g indicates energy bandgap of layers and obtained from Tauc curves; VBM indicates valence band maximum; W_s indicates the work function of layers; E_c indicates conduction band edge; E_v refers valence band edge

Sample name	E_g (eV)	VBM (eV)	W_s (eV)	E_v (eV)	E_c (eV)
Control	1.53	−1.61	−3.88	−5.49	−3.96
CTABr-0%	1.54	−1.60	−3.81	−5.41	−3.87
CTABr-5%	1.54	−1.65	−3.72	−5.37	−3.83

enlarged perovskite grains (see Fig. 4).[30,31] Higher V_{OC} and FF recorded for the CTABr-5% PSCs are due to longer carriers' lifetime measured in them.

Fig. 6(b) shows the C^{-2}–V curves for control, CTABr-0%, and CTABr-5% FAPbI₃ PSCs. The Mott–Schottky formula (eqn (2)) was employed for fitting C^{-2}–V curves to measure built-in potential (V_{bi}) in the depletion region:

$$C^{-2} = \frac{-2}{A^2 e N \varepsilon_0 \varepsilon_r}\left(V + \frac{2K_B T}{e} - V_{bi}\right) \quad (2)$$

In eqn (2), A is the PSCs' active area, N is carrier density, e is electron charge, K_B is Boltzmann constant, T is temperature of test condition, V is applied voltage, ε_0 is vacuum permittivity, and ε_r is dielectric constant of FAPbI₃. As specified in C^{-2}–V plots, the CTABr vapor enhances V_{bi} of FAPbI₃ PSCs from 0.83 V to 0.94 V. In the next step, applying CTABr + 5% KSCN vapor on the FAPbI₃ layer improves V_{bi} up to 1.01 V. The boosted V_{bi} in FAPbI₃ PSCs implies to a stronger driving force to charge

separation, resulting in increased carrier extraction to electrodes and enhanced J_{SC}.

In addition, the ultraviolet photoelectron spectroscopy (UPS) test was utilized to investigate the possible band alignment phenomenon between energy levels of different FAPbI₃ layers
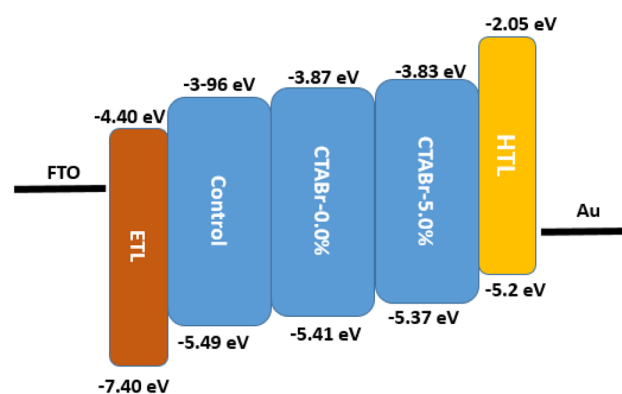

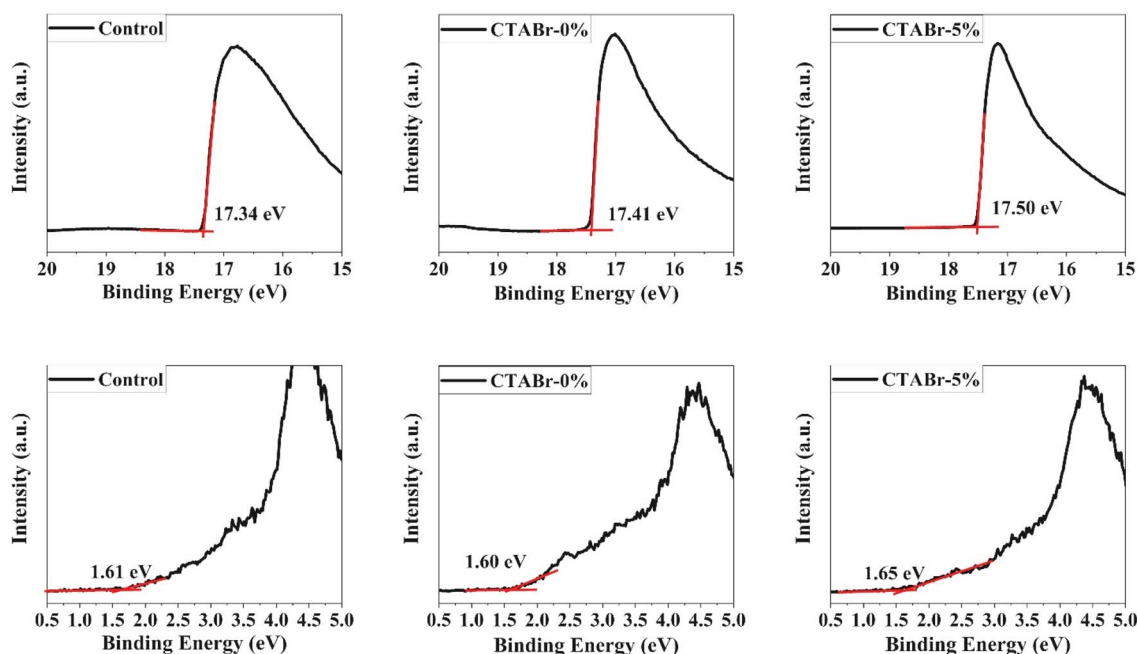**Fig. 8** Impact on band positioning after vapor treatment.

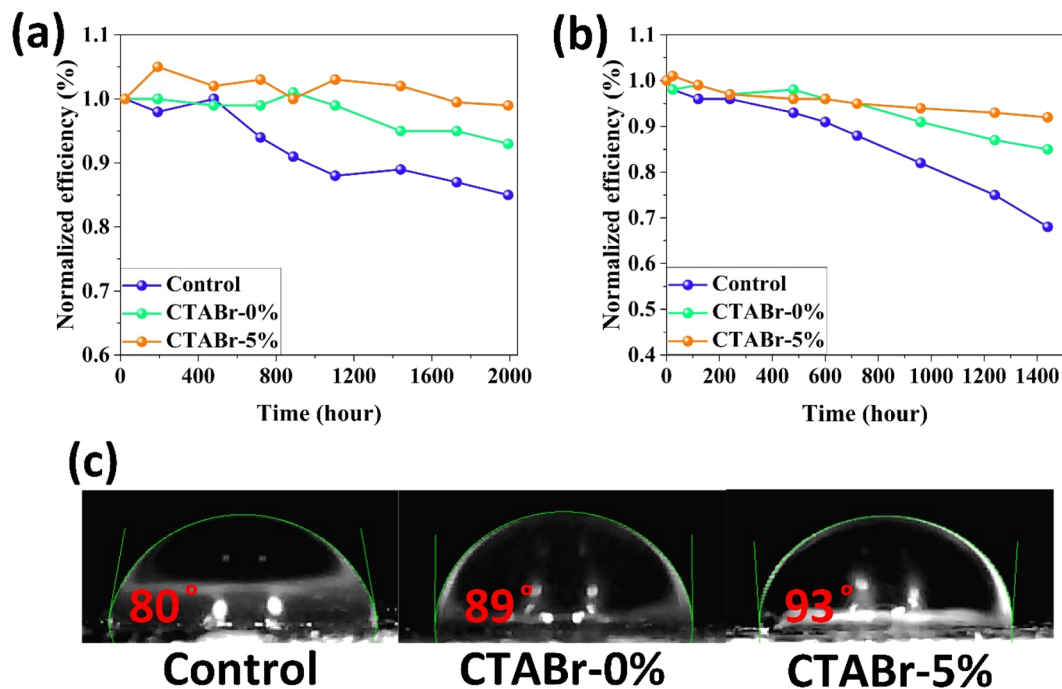**Fig. 7** UPS spectrum of control, CTABr-0%, and CTABr-5% FAPbI₃ films.

Fig. 9 Efficiency tracking of the unsealed FAPbI$_3$ solar cells based on control, CTABr-0%, and CTABr-5% FAPbI$_3$ layers in (a) a dry box with humidity level of lower than 20%, and in (b) ambient air with relative humidity of 40−50% at room temperature in dark condition. (c) Water droplet angle on the control, CTABr-0%, and CTABr-5% FAPbI$_3$ layers.

and HTL. The UPS spectra are depicted in Fig. 7 and the analyzed results are summarized in Table 3. The valence band of control, CTABr-0%, and CTABr-5% FAPbI$_3$ layers are −5.49, −5.41, and −5.37 eV. The valence band energy reported for spiro-OMeTAD is −5.2 eV.[32,33] Therefore, the CTABr + 5% KSCN vapor nears the valence band energy of FAPbI$_3$ to the spiro-OMeTAD value and enhances the hole transfer from the FAPbI$_3$ to HTL along with preventing the electron transportation at the interface of FAPbI$_3$/HTL. The impact of vapor treatment on band positioning of perovskite layer is shown in Fig. 8.

In the end, we conducted stability tests in two environments with relative humidity levels of <20% (Fig. 9(a)) and 40−50% (Fig. 9(b)) to investigate the effects of the vapor treatment approach on the stability behavior of FAPbI$_3$ layers. Among control, CTABr-0%, and CTABr-5% PSCs, the CTABr-5% device shows higher shelf stability, remaining 99% of its initial efficiency during 1992 h aging time, higher than 93% in the CTABr-0% and 85% in the control devices (see Fig. 9(a)). Higher shelf stability observed in the CTABr-5% FAPbI$_3$ correlates with higher phase and structural stabilities in the CTABr-5% FAPbI$_3$, which is supported by its intensified α-phase (see Fig. 3(d)). In addition, CTABr-5% FAPbI$_3$ device shows higher resistance against humidity than the other devices. The CTABr-5% device keeps 92% of its initial efficiency after 1440 h, while CTABr-0% and control devices keep 85% and 68% of their efficiency during stability test (see Fig. 9(b)). Fig. 9(c) shows the contact angle of water droplets on the control, CTABr-0%, and CTABr-5% FAPbI$_3$ layers. Contact angles are 80°, 89°, and 93°. The enlarged contact angle achieved for the CTABr-5% refers to its improved

humidity resistance.[34] The hydrophobic nature of the long chain CTABr material brings a waterproof FAPbI$_3$ layer and prevents FAPbI$_3$ degradation. The passivated Gbs is another reason for the higher humidity stability observed in the CTABr-5% FAPbI$_3$ PSCs.[35,36]

4. Conclusion

We introduced a vapor-based treatment approach to modify FAPbI$_3$ formation and fabricate a pure α-FAPbI$_3$ phase perovskite layer. During the fabrication process of the FAPbI$_3$ layer, we vaporized the CTABr + 5% KSCN on it. This way improved the PV efficiency and stability of fabricated PSCs. It was observed that the vapor of CTABr + 5% KSCN simultaneously enlarges FAPbI$_3$ grains and passivates perovskite Gbs. It generates a favorable FAPbI$_3$ layer for solar cell devices. The vapor treatment step reduces the trap-assisted charge recombination in the FAPbI$_3$ layer and elongates the carriers' lifetime. In addition, a band alignment occurred between the valence band of FAPbI$_3$ and HTL, resulting in facilitated hole transfer at FAPbI$_3$/HTL interface. As a result, the CTABr + 5% KSCN vapor fabricates PSCs with a champion efficiency of 22.34%, higher than the efficiency of 19.48% for the control PSCs. In addition, the CTABr-5% FAPbI$_3$ solar cells had higher structural and humidity stabilities than the control devices.

Conflicts of interest

The authors declare that they have no conflict of interest.

References

1 H. Min, D. Y. Lee, J. Kim, G. Kim, K. S. Lee, J. Kim, M. J. Paik, Y. K. Kim, K. S. Kim and M. G. Kim, Perovskite solar cells with atomically coherent interlayers on SnO_2 electrodes, *Nature*, 2021, **598**, 444–450.

2 H. R. Mohseni, M. Dehghanipour, N. Dehghan, F. Tamaddon, M. Ahmadi, M. Sabet and A. Behjat, Enhancement of the photovoltaic performance and the stability of perovskite solar cells *via* the modification of electron transport layers with reduced graphene oxide/polyaniline composite, *Sol. Energy*, 2021, **213**, 59–66.

3 J. Jeong, M. Kim, J. Seo, H. Lu, P. Ahlawat, A. Mishra, Y. Yang, M. A. Hope, F. T. Eickemeyer and M. Kim, Pseudo-halide anion engineering for α-FAPbI 3 perovskite solar cells, *Nature*, 2021, **592**, 381–385.

4 H. Min, M. Kim, S.-U. Lee, H. Kim, G. Kim, K. Choi, J. H. Lee and S. I. Seok, Efficient, stable solar cells by using inherent bandgap of α-phase formamidinium lead iodide, *Science*, 2019, **366**, 749–753.

5 H. Lu, Y. Liu, P. Ahlawat, A. Mishra, W. R. Tress, F. T. Eickemeyer, Y. Yang, F. Fu, Z. Wang and C. E. Avalos, Vapor-assisted deposition of highly efficient, stable black-phase $FAPbI_3$ perovskite solar cells, *Science*, 2020, **370**, eabb8985.

6 T. M. Koh, K. Fu, Y. Fang, S. Chen, T. C. Sum, N. Mathews, S. G. Mhaisalkar, P. P. Boix and T. Baikie, Formamidinium-containing metal-halide: an alternative material for near-IR absorption perovskite solar cells, *J. Phys. Chem. C*, 2014, **118**, 16458–16462.

7 M. K. A. Mohammed, A. E. Shalan, M. Dehghanipour and H. R. Mohseni, Improved mixed-dimensional 3D/2D perovskite layer with formamidinium bromide salt for highly efficient and stable perovskite solar cells, *Chem. Eng. J.*, 2022, **428**, 131185.

8 T. Bu, X. Liu, Y. Zhou, J. Yi, X. Huang, L. Luo, J. Xiao, Z. Ku, Y. Peng and F. Huang, A novel quadruple-cation absorber for universal hysteresis elimination for high efficiency and stable perovskite solar cells, *Energy Environ. Sci.*, 2017, **10**, 2509–2515.

9 K. M. Reza, A. Gurung, B. Bahrami, A. H. Chowdhury, N. Ghimire, R. Pathak, S. I. Rahman, M. A. R. Laskar, K. Chen and R. S. Bobba, Grain Boundary Defect Passivation in Quadruple Cation Wide-Bandgap Perovskite Solar Cells, *Sol. RRL*, 2021, **5**, 2000740.

10 E. Gutierrez-Partida, H. Hempel, S. Caicedo-Davila, M. Raoufi, F. Pena-Camargo, M. Grischek, R. Gunder, J. Diekmann, P. Caprioglio and K. O. Brinkmann, Large-grain double cation perovskites with 18 μs lifetime and high luminescence yield for efficient inverted perovskite solar cells, *ACS Energy Lett.*, 2021, **6**, 1045–1054.

11 X. X. Gao, W. Luo, Y. Zhang, R. Hu, B. Zhang, A. Züttel, Y. Feng and M. K. Nazeeruddin, Stable and high-efficiency methylammonium-free perovskite solar cells, *Adv. Mater.*, 2020, **32**, 1905502.

12 E. Smecca, Y. Numata, I. Deretzis, G. Pellegrino, S. Boninelli, T. Miyasaka, A. La Magna and A. Alberti, Stability of solution-processed MAPbI 3 and FAPbI 3 layers, *Phys. Chem. Chem. Phys.*, 2016, **18**, 13413–13422.

13 Z. Shao, H. Meng, X. Du, X. Sun, P. Lv, C. Gao, Y. Rao, C. Chen, Z. Li and X. Wang, Cs4PbI6-Mediated Synthesis of Thermodynamically Stable FA0. 15Cs0. $85PbI_3$ Perovskite Solar Cells, *Adv. Mater.*, 2020, **32**, 2001054.

14 L. Gil-Escrig, C. Dreessen, F. Palazon, Z. Hawash, E. Moons, S. Albrecht, M. Sessolo and H. J. Bolink, Efficient wide-bandgap mixed-cation and mixed-halide perovskite solar cells by vacuum deposition, *ACS Energy Lett.*, 2021, **6**, 827–836.

15 G. Kim, H. Min, K. S. Lee, D. Y. Lee, S. M. Yoon and S. I. Seok, Impact of strain relaxation on performance of α-formamidinium lead iodide perovskite solar cells, *Science*, 2020, **370**, 108–112.

16 N. Rolston, K. A. Bush, A. D. Printz, A. Gold-Parker, Y. Ding, M. F. Toney, M. D. McGehee and R. H. Dauskardt, Engineering stress in perovskite solar cells to improve stability, *Adv. Energy Mater.*, 2018, **8**, 1802139.

17 B.-w. Park, H. W. Kwon, Y. Lee, D. Y. Lee, M. G. Kim, G. Kim, K.-j. Kim, Y. K. Kim, J. Im and T. J. Shin, Stabilization of formamidinium lead triiodide α-phase with isopropylammonium chloride for perovskite solar cells, *Nat. Energy*, 2021, **6**, 419–428.

18 Y. Liu, S. Akin, A. Hinderhofer, F. T. Eickemeyer, H. Zhu, J. Y. Seo, J. Zhang, F. Schreiber, H. Zhang and S. M. Zakeeruddin, Stabilization of highly efficient and stable phase-pure $FAPbI_3$ perovskite solar cells by molecularly tailored 2D-overlayers, *Angew. Chem., Int. Ed.*, 2020, **59**, 15688–15694.

19 S. Jeong, S. Seo, H. Yang, H. Park, S. Shin, H. Ahn, D. Lee, J. H. Park, N. G. Park and H. Shin, Cyclohexylammonium-Based 2D/3D Perovskite Heterojunction with Funnel-Like Energy Band Alignment for Efficient Solar Cells (23.91%), *Adv. Energy Mater.*, 2021, 2102236.

20 C. Shen, Y. Wu, S. Zhang, T. Wu, H. Tian, W.-H. Zhu and L. Han, Stabilizing formamidinium lead iodide perovskite by sulfonyl-functionalized phenethylammonium salt *via* crystallization control and surface passivation, *Sol. RRL*, 2020, **4**, 2000069.

21 M. Martynow, D. Głowienka, Y. Galagan and J. Guthmuller, Effects of Bromine Doping on the Structural Properties and Band Gap of CH_3NH_3Pb $(I_{1−x}Br_x)$ 3 Perovskite, *ACS Omega*, 2020, **5**, 26946–26953.

22 F. Peña-Camargo, P. Caprioglio, F. Zu, E. Gutierrez-Partida, C. M. Wolff, K. Brinkmann, S. Albrecht, T. Riedl, N. Koch and D. Neher, Halide segregation *versus* interfacial recombination in bromide-rich wide-gap perovskite solar cells, *ACS Energy Lett.*, 2020, **5**, 2728–2736.

23 M. Dehghanipour, A. Behjat and H. A. Bioki, Fabrication of stable and efficient 2D/3D perovskite solar cells through post-treatment with $TBABF_4$, *J. Mater. Chem. C*, 2021, **9**, 957–966.

24 S. Tan, I. Yavuz, M. H. Weber, T. Huang, C.-H. Chen, R. Wang, H.-C. Wang, J. H. Ko, S. Nuryyeva and J. Xue, Shallow iodine defects accelerate the degradation of α-phase formamidinium perovskite, *Joule*, 2020, **4**, 2426–2442.

25 C. Yang, H. Wang, Y. Miao, C. Chen, M. Zhai, Q. Bao, X. Ding, X. Yang and M. Cheng, Interfacial molecular doping and energy level alignment regulation for perovskite solar cells with efficiency exceeding 23, *ACS Energy Lett.*, 2021, **6**, 2690–2696.

26 T. Zhou, H. Lai, T. Liu, D. Lu, X. Wan, X. Zhang, Y. Liu and Y. Chen, Highly efficient and stable solar cells based on crystalline oriented 2D/3D hybrid perovskite, *Adv. Mater.*, 2019, **31**, 1901242.

27 F. Xu, J. Liu, A. S. Subbiah, W. Liu, J. Kang, G. T. Harrison, X. Yang, F. H. Isikgor, E. Aydin and M. De Bastiani, Potassium Thiocyanate-Assisted Enhancement of Slot-Die-Coated Perovskite Films for High-Performance Solar Cells, *Small Sci.*, 2021, **1**, 2000044.

28 J.-W. Lee, S. Tan, T.-H. Han, R. Wang, L. Zhang, C. Park, M. Yoon, C. Choi, M. Xu and M. E. Liao, Solid-phase hetero epitaxial growth of α-phase formamidinium perovskite, *Nat. Commun.*, 2020, **11**, 1–11.

29 F. Li, X. Deng, F. Qi, Z. Li, D. Liu, D. Shen, M. Qin, S. Wu, F. Lin and S.-H. Jang, Regulating surface termination for efficient inverted perovskite solar cells with greater than 23% efficiency, *J. Am. Chem. Soc.*, 2020, **142**, 20134–20142.

30 G. Nagaraj, M. K. A. Mohammed, M. Shekargoftar, P. Sasikumar, P. Sakthivel, G. Ravi, M. Dehghanipour, S. Akin and A. E. Shalan, High-performance perovskite solar cells using the graphene quantum dot-modified SnO$_2$/ZnO photoelectrode, *Mater. Today Energy*, 2021, **22**, 100853.

31 H. Su, J. Zhang, Y. Hu, X. Du, Y. Yang, J. You, L. Gao and S. Liu, Fluoroethylamine Engineering for effective passivation to attain 23.4% efficiency perovskite solar cells with superior stability, *Adv. Energy Mater.*, 2021, **11**, 2101454.

32 Z. He, Y. Zhou, C. Xu, Y. Su, A. Liu, Y. Li, L. Gao and T. Ma, Mechanism of Enhancement in Perovskite Solar Cells by Organosulfur Amine Constructed 2D/3D Heterojunctions, *J. Phys. Chem. C*, 2021, **125**, 16428–16434.

33 E. Akman and S. Akin, Poly(N,N′-bis-4-butylphenyl-N,N′-bisphenyl) benzidine-based interfacial passivation strategy promoting efficiency and operational stability of perovskite solar cells in regular architecture, *Adv. Mater.*, 2021, **33**, 2006087.

34 Y. Zhang, Y. Li, L. Zhang, H. Hu, Z. Tang, B. Xu and N. G. Park, Propylammonium Chloride Additive for Efficient and Stable FAPbI$_3$ Perovskite Solar Cells, *Adv. Energy Mater.*, 2021, 2102538.

35 M. Dehghanipour, A. Behjat, A. Shabani and M. Haddad, Toward desirable 2D/3D hybrid perovskite films for solar cell application with additive engineering approach, *J. Mater. Sci.: Mater. Electron.*, 2022, 1–12.

36 S. Tan, I. Yavuz, N. De Marco, T. Huang, S. J. Lee, C. S. Choi, M. Wang, S. Nuryyeva, R. Wang and Y. Zhao, Steric impediment of ion migration contributes to improved operational stability of perovskite solar cells, *Adv. Mater.*, 2020, **32**, 1906995.